X-Ray Scattering Study of Restacking Transitions in the Crystalline-B Phases of Heptyloxybenzylidene Heptylaniline (70.7)

X-ray scattering study of restacking transitions in the crystalline-*B* phases of heptyloxybenzylidene heptylaniline (7O.7)

Jeffrey Collett,* L. B. Sorensen,† and P. S. Pershan
Division of Applied Sciences, Harvard University, Cambridge, Massachusetts 02138

J. Als-Nielsen
Risø National Laboratory, DK-4000 Roskilde, Denmark
(Received 28 January 1985)

This paper reports a comprehensive x-ray diffraction study of the structure and the restacking transitions which occur within the crystalline-*B* phases of N-[4-(*n*-heptyl)oxybenzylidene]-4′-(*n*-heptyl)aniline (7O.7). Between 63 °C and 59 °C, this system exhibits a rich structural behavior with a series of three transitions involving restacking and subtle changes in the intralayer packing. In order of decreasing temperature, the structures are hexagonal close packed (69—63 °C), orthorhombic *F* (63—60.1 °C), monoclinic *C* (60.1—59.75 °C), and simple hexagonal (59.75—55 °C). In the last three phases, there is also a long-wavelength modulation ($\lambda \sim 100$ Å) in which the smectic layers are displaced along their normals. The wave vector of the modulation lies in the plane of the smectic layers directed along a reciprocal-lattice vector and exhibits a weak (~20%) temperature variation. Both low-resolution (rotating-anode) and high-resolution (synchrotron) measurements of the structures and of the diffuse scattering are reported.

I. INTRODUCTION

Interest in the properties of smectic-*B* phases has been greatly stimulated by recent theoretical and experimental developments. Since the smectic phases have extremely weak interlayer coupling and a variety of two-dimensional (2D) intralayer structures, they have become particularly valuable models for the study of weakly interacting 2D systems. Recent advances in the theory of melting in two dimensions[1] have led to theoretical models of the smectic-*B* phase based on weakly coupled two-dimensional systems.[2–4] One of these models predicted two possible smectic-*B* phases: a crystalline-*B* phase with true long-range positional and orientational order and a three-dimensional (3D) hexatic-*B* phase consisting of coupled 2D hexatic layers.[4] The 3D hexatic phase does not have long-range positional order, but does possess long-range order in bond-angle orientation.

Early low-resolution x-ray studies of several smectic-*B* materials indicated that the smectic-*B* phase had a structure corresponding to the hexatic-*B* phase.[5] However, later experiments showed that although the original materials actually had crystalline-*B* order, both kinds of order occur, with the crystalline-*B* order occurring much more often than the hexatic-*B* order.[6–10] The resolution of the original controversy was due to both high-resolution x-ray diffraction measurements and to the use of freely-suspended liquid-crystal films.[6,8]

The measurements made on the crystalline-*B* materials showed a variety of unusual features due to the weak coupling between layers which makes these quasi-2D phases extremely interesting in their own right. X-ray diffraction experiments have revealed strong diffuse-scattering modes which can be interpreted as low-energy phonons with polarizations in the plane of the smectic layers and wave vectors normal to the smectic layers.[7,8] This strong diffuse scattering and the poor sample mosaic found in the earlier experiments hindered the identification of these materials as true 3D crystals. The second feature observed in these systems is the preponderance of restacking transitions involving dramatic shifts in the relative positions of adjacent layers.[6,9,11–13] Prior to the present study, no latent heat or other thermal anomaloy had been observed in conjunction with the restacking transitions, leaving their detailed nature unknown. High-resolution ac calorimetry measurements,[14] motivated by our initial publication of the restacking-transition sequence in 7O.7,[15] verified the presence of the weak first-order transitions observed in this study. The third feature of these phases which merits closer examination is the presence of modulations polarized normal to the layers with wave vectors in the plane of the layers.[9,11,13]

In this study we carefully examined freely-suspended crystalline-*B* films of N-[4-(*n*-heptyl)oxybenzylidene]-4′-(*n*-heptyl)aniline (7O.7). The crystalline-*B* phases were originally thought to consist of just the two hexagonal-close-packed structures with *ABAB* and *ABCABC* stacking; subsequently, phases with *AAA* stacking were suggested by Gane, Leadbetter and Wrighton.[9] Prior to the present study, the crystalline-*B* phase of 7O.7 has been identified as a hexagonal-close-packed structure with *ABAB* stacking and with layer modulations observed in the low-temperature region of the phase.[11–13] We found that the crystalline-*B* phase of 7O.7 actually has four distinct crystal structures separated by three restacking transitions;[15,16] these phases (in order of decreasing temperature) are the following: a hexagonal-close-packed structure (hcp) with *ABAB* stacking, an orthorhombic-face-centered structure (ortho-*F*), a monoclinic-*C*-centered structure (mono-*C*), and a simple hexagonal structure.

We also found that the last three of these structures possess a one-dimensional modulation of the smectic layers with a single (temperature-dependent) wave vector in the direction of the molecular motion at the transition from the hcp to the ortho-F structure.

II. EXPERIMENTAL TECHNIQUES

Two techniques were crucial in developing the present understanding of the microscopic structure of smectic-B phases; both freely suspended liquid-crystal film techniques and high-resolution x-ray diffraction techniques allowed the unambiguous determination of these structures. High-resolution diffraction clearly distinguishes between crystalline phases with true long-range order and disordered phases with abnormally long correlation lengths. This was crucial in the experiments of Pershan *et al.*[7] on bulk samples, and of Moncton and Pindak[6,8] on freely-suspended films, in which the smectic-B phase of N-[4-(n-butyl)oxybenzylidene]-4'-(n-octyl)aniline (4O.8) was unambiguously shown to be crystalline. The freely-suspended-film technique allows the preparation of single-crystal domains with lateral dimensions of 1 mm or more and allows a study of the interlayer correlations uncomplicated by the problem of sample mosaic.[6] This was crucial for the present study of the rich crystallography of the crystalline-B phases of 7O.7. In this section the details of the x-ray spectrometers used in the present measurements and a description of the free-film x-ray oven are presented.

High-resolution x-ray measurements were carried out using synchrotron radiation and the triple-axis spectrometer at the Hamburger Synchrotronstrahlungslabor, Deutschis Elektronen-Synchrotron (HASYLAB) in Hamburg, Germany. Single-crystal Ge(111) reflections were used in the monochromator and analyzer. The wavelength was chosen to be 1.5 Å. For the in-plane scattering angle of 20° appropriate for 7O.7, this spectrometer configuration had a longitudinal resolution of 6×10^{-4} Å^{-1} and a transverse resolution of $\sim1\times10^{-4}$ Å^{-1} [full width at half maximum (FWHM)]. This resolution allowed the measurement of correlation lengths up to 1 μm and the determination of lattice-constant differences to better than one part in 10^4. Absolute lattice-constant measurements were not as good due to systematic drifts in the x-ray wavelength with time. The vertical resolution of the spectrometer was determined by the vertical acceptance of the detector and was varied from 8×10^{-4} to 4×10^{-2} Å^{-1}, with a slit at the detector position.

Lower-resolution data were taken on similar spectrometers at Harvard University and the Massachusetts Institute of Technology (MIT) using Cu $K\alpha$ radiation from rotating-anode sources and highly oriented pyrolytic-graphite (002) reflections in the monochromator and analyzer. For these spectrometers, the longitudinal and transverse resolutions were 3.5×10^{-2} Å^{-1} and 6.3×10^{-3} Å^{-1} (FWHM), respectively. The vertical resolution was determined by slits and was varied from 7×10^{-2} to 3×10^{-1} Å^{-1}. Some low-resolution measurements were also made at MIT using a pyrolytic-graphite monochromator and a TEC model-210 linear position-sensitive proportional counter. The longitudinal resolution in this case was about a factor of 4 better than that obtained with graphite monochromator and analyzer crystals.

All of these spectrometers were two-circle (planar) instruments. In order to observe the diffraction from the single-crystal samples, it was necessary to introduce a rotation stage inside the liquid-crystal oven to allow the desired Bragg vector of the crystal to be brought into the scattering plane of the spectrometer. This rotation stage has its axis of rotation normal to the smectic layers and in the scattering plane of the two-circle diffractometer. The two-circle diffractometer allowed us to perform scans along q_z (normal to the smectic layers) and along q_{xy} (parallel to the smectic-layer planes). The internal rotation stage controlled the angle χ which determined the direction of q_{xy} within the smectic layers.

The oven used in these experiments had to satisfy a number of design criteria.[16] The four major requirements were: millikelvin temperature stability, extremely low-background scattering, the ability to make films and measure their thickness while in place, and the incorporation of the necessary remotely controlled χ rotational degree of freedom described above. In addition to these features, provisions were made to mount samarium-cobalt permanent magnets inside the rotation circle to allow magnetic orientation of the director for smectic phases in which the long axis of the molecules is tilted with respect to the layer normal.

Since the samples used in these experiments were thin films, it was necessary to reduce the background scattering as much as possible. To accomplish this, the region around the sample from which a photon from the direct beam can be scattered into the detector should contain no scatterers except the sample. This region is referred to as the scattering volume and should not contain any windows or air. For this reason, the oven was designed for vacuum operation. Pressures of 10^{-1} Torr obtained with a mechanical roughing pump were adequate for all of the present measurements. In practice, the presence of air (at 1 atm) did not cause a significant background problem in the measurement of films several hundred layers thick. However, the background had to be reduced to perform measurements on thin films.

The general layout of the oven is shown in Fig. 1. The oven consists of two concentric cylindrical brass cans with the inner can heated and insulated from the outer can by vacuum and by Delrin support posts. Heaters on the top and bottom plates of the inner can could be independently adjusted to minimize temperature gradients. The outer can is sealed using O-ring seals. An Ardel kinematics rotation stage is rigidly suspended from the inner cover by a brass plate [Fig. 1(a)]. A cross section of the rotation stage in the plane normal to the rotation axis of the stage is shown in Fig. 1(b). The drive shaft from this stage is coupled to the rotary-vacuum feedthrough in the outer cover by a stainless-steel bellows which takes up mechanical stresses and provides thermal isolation from the outside environment. The rotation stage is driven by a computer-controlled stepping motor mounted on top of the oven. A cylindrical beryllium window in the inner can and a corresponding Kapton window in the outer can provide 300° x-ray access in the scattering plane.

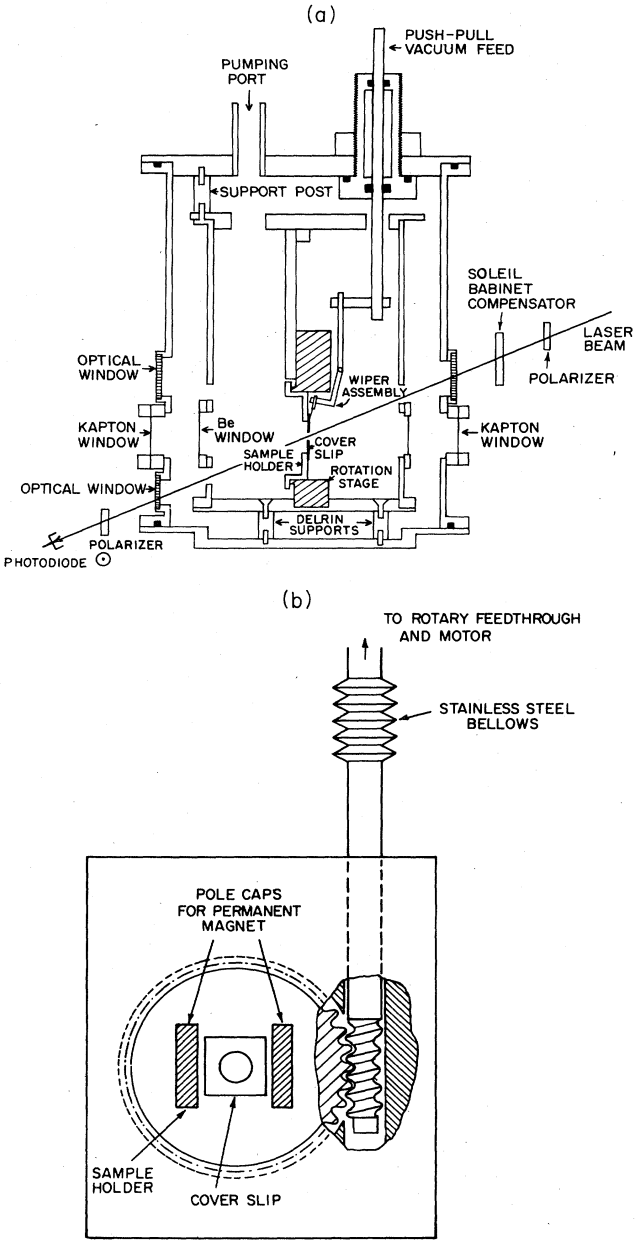

FIG. 1. (a) Schematic cross section of the free-film oven. (b) Cross section of the rotation stage normal to its axis of rotation. (The soft-iron return path for the permanent magnet is not shown.)

Films were produced on a sample holder mounted in the 2-in.-diam aperture in the rotation stage. As in the other free-film experiments,[6,17] the films were produced by pulling a microscope cover slip (attached to the wiper assembly) across a polished hole in a second cover slip mounted in the rotation stage. For these experiments, we used a 7-mm-diam round hole in a 0.2-mm-thick glass cover slip. Permanent magnets mounted in a soft-iron sample holder provide a magnetic field in the plane of the cover slip [Fig. 1(b)]. Before closing the oven, a small amount of the liquid-crystal compound was melted around the edge of the hole. The oven was then sealed, evacuated, and heated to bring the sample into the smectic-A phase. The first cover slip was then drawn across the second via a push-pull vacuum feedthrough; the liquid crystal then spontaneously produced a free film across the open hole (like a soap bubble). Films were produced repeatedly until one of the desired thickness was obtained.

A birefringence measurement was used to determine the film thickness; the simple reflectivity technique used in previous studies of thin films is only useful up to thicknesses of about 25 layers where the reflectivity reaches its first maximum. The birefringence method was better for thick films because the optical phase retardation is a single-valued function over the entire range of thicknesses of interest (50—1000 layers) whereas the reflectivity goes through many maxima and minima. Optical access to the film was provided by three fused-quartz windows adjacent to the x-ray window in the outer can. A He-Ne laser beam was incident as shown in Fig. 1(a) with its polarization at a 45° angle to the optic axes of the liquid-crystal film. A Soleil-Babinet compensator was placed in the beam with its axes parallel to those of the film. By adjusting the compensator to minimize the transmission of the beam through the set of crossed polarizers, the optical phase retardation introduced by the film could be determined. Using estimated values for the refractive indices of 7O.7,[18] the film thickness could then be calculated. The film thicknesses obtained using this method were uncertain by about 20% due to the uncertainty in the refractive-index values. Thin-film thicknesses were determined using the standard reflectivity method.

In order to accurately determine the temperature of thin films, it is necessary to surround the sample with a very uniform temperature distribution. Since the heat flow through the film to the supporting cover slip and rotation stage is proportional to the thickness of the film, while the radiative and conductive heat flow from the film surface to the oven walls scales with the surface area, the surface terms will eventually dominate the thermal transport for thin enough films. In our evacuated oven, the heat flow was dominated by line-of-sight conduction and radiation to the oven walls nearest the film. For this reason we used beryllium (a good thermal conductor) windows near the sample and carefully balanced the power to the heaters to minimize the gradient between the rotation stage and the surrounding walls. In addition, the optical windows were designed to subtend the smallest solid angle which would still allow the necessary thickness measurements.

The overall temperature stability of the oven was very good. Short-term stability (20 min) of better than 1 mK was typical. The behavior over longer periods depended on the temperature stability of the laboratory. For typical variations in the room temperature of less than 3 °C, the oven was stable to better than 5 mK for many hours. One of the reasons for the excellent short-term stability was the massiveness of the inner-oven assembly. This resulted in good stability but slow response; the full equilibration time (to ± 5 mK) was about 2 h under vacuum conditions.

III. EXPERIMENTAL RESULTS

These studies have revealed an unusually rich structural behavior within the crystalline-B range ($69\,^{\circ}\mathrm{C} > T > 55\,^{\circ}\mathrm{C}$) with a series of three first-order transitions between 63 °C and 59 °C that involve restacking of the layers and subtle changes in the intralayer packing. In order of decreasing temperature, the system goes from a hexagonal-close-packed structure (hcp) with $ABAB$ stacking (hcp, $69\,^{\circ}\mathrm{C} > T > 63\,^{\circ}\mathrm{C}$) to an orthorhombic-face-centered structure (ortho-F, $63\,^{\circ}\mathrm{C} > T > 60.1\,^{\circ}\mathrm{C}$), a monoclinic-$C$-centered phase (mono-$C$, $60.1\,^{\circ}\mathrm{C} > T > 59.75\,^{\circ}\mathrm{C}$), and a simple hexagonal structure (hex-AA, $59.75\,^{\circ}\mathrm{C} > T > 55\,^{\circ}\mathrm{C}$). At 55 °C, 7O.7 transforms into a smectic-G phase, a crystalline, mono-C-centered structure with the long axes of the molecules tilted by 23° with respect to the normals to the smectic layers.[9,13] The ortho-F, mono-C, and hex-AA phases all exhibit a one-dimensional modulation of the smectic layers in which the displacement is normal to the layers and the modulation wave vector is in the plane of the layers. (See Note added in proof below.)

The relative stacking of the adjacent layers in these phases is shown in Fig. 2. The primitive real and reciprocal lattices for the three lowest-temperature phases are also given. The modulation wave vector is directed along the y direction. In order to present the data in a unified form, all the peaks have been indexed by the reciprocal lattice which uses the in-plane (x,y) components of the $\mathbf{b}_1$ and $\mathbf{b}_2$ to form a lattice which is the reciprocal of the lattice of the individual layers. The third reciprocal-lattice vector was chosen along the z direction with a length equal to 2π/(molecular length). Although the peaks no longer occur only at integer values, this description clearly separates the changes in the intralayer packing (apparent in $\mathbf{b}_{1xy}$ and $\mathbf{b}_{2xy}$) from the changes in the stacking (reflected by changes in the period and displacements along the z direction).

At temperatures between 63 °C and 69 °C, 7O.7 exhibited the $ABAB$-stacked hcp structure common in crystalline-B materials. Scans along q_z through the six lowest-order in-plane peaks showed peaks at integral and half-integral multiples of $2\pi/c$ (where c is the smectic layer spacing). The observed peaks at the half-integral positions were three times as intense as the peaks at the integral positions as expected from the calculated structure factor (after correcting for the form factor and the Debye-Waller effects). Figure 3(a) shows a low-resolution q_z scan in this phase.

At 63 °C there was an abrupt first-order transition to an ortho-F phase. This phase can be described by the primitive triclinic unit cell of the lattice in Fig. 2, or by a larger orthorhombic cell. The choice $s = \frac{1}{2}$ for the representation in Fig. 2 produces the orthorhombic unit cell. When freely-suspended films in the ortho-F phase were cooled slowly through the transition into the hex-AA phase and were then heated slowly back into the ortho-F phase, large single domains were formed. Figures 3(b) and 3(d) show low-resolution q_z scans through $\mathbf{b}_1$ and $\mathbf{b}_2$. The high-resolution synchrotron measurements showed that the direct lattice was compressed along y and was extended along x. Because of this distortion, the magnitudes of $\mathbf{b}_1$ and $\mathbf{b}_2$ were different; the synchrotron measurements of the distortion as a function of temperature are shown in Fig. 4(a). This distortion is parametrized by ϵ_x and ϵ_y in the representation in Fig. 2; the measured distortion was consistent with an area-conserving change with $\epsilon_x = \epsilon_y = 10^{-3}$. This structure has not previously been associated with crystalline-B phases because the distortion is extremely small. The use of freely-suspended films together with the high resolution provided by the HASYLAB spectrometer were crucial for the identification of this phase. The free-film technique allowed the preparation of large single-domain samples which were not available using standard sample-preparation techniques. In a normal sample which has many domains, the peak locations along q_z are the same for the ortho-F and

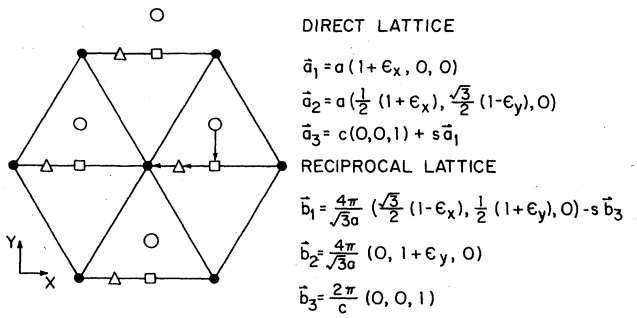

FIG. 2. Relative positions of the adjacent layers in the various phases: solid circles, reference layer position; open circles, hexagonal close packed; squares, ortho-F; and triangles, mono-C. In the hex-AA phase the adjacent-layer position coincides with the reference layer. The primitive unit cells for the real and reciprocal lattices of the ortho-F, mono-C, and hex-AA structures are shown on the right.

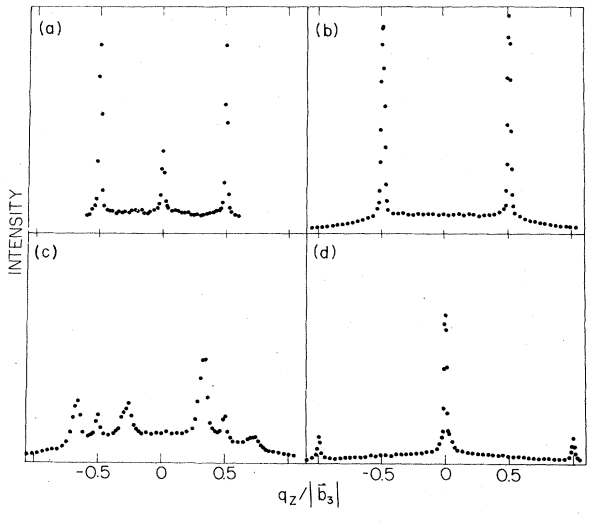

FIG. 3. Low-resolution q_z scans: (a) through an in-plane peak for $T > 63\,^{\circ}\mathrm{C}$ ($T = 65.43\,^{\circ}\mathrm{C}$); (b) through $\mathbf{b}_1$ in the ortho-F phase at $T = 60.88\,^{\circ}\mathrm{C}$; (c) through $\mathbf{b}_1$ in the mono-C phase at $T = 60.02\,^{\circ}\mathrm{C}$; (d) through $\mathbf{b}_2$ in the hex-AA phase at $T = 59.35\,^{\circ}\mathrm{C}$; identical scans through $\mathbf{b}_2$ are found in both the ortho-F and mono-C phases.

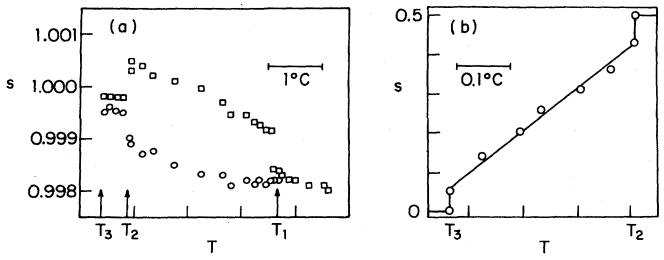

FIG. 4. (a) Measurement of distortion in intralayer packing: circles, $|\mathbf{b}_1|$; squares, $|\mathbf{b}_2|$. Data are plotted in units for s of $4\pi/\sqrt{3}a = 1.434$ Å^{-1}. Transition temperatures are marked: T_1, hcp to ortho-F; T_2, ortho-F to mono-C; T_3, mono-C to hex-AA. (b) Adjacent layer displacement versus temperature in the mono-C phase.

the hcp structures. Consequently, although the relative intensities are quite different (the half-integer peaks are twice as intense as the integer-order peaks in the ortho-F phase instead of the threefold ratio found in the hcp phase), it is still extremely difficult to distinguish these two phases in a low-resolution measurement. At high resolution, the phases can be distinguished by the distortion of the intralayer packing mentioned above; this is how the phase was originally identified using polydomain samples at HASYLAB before the technique for producing monodomain samples was discovered.

At $T = 60.1$ °C, the ortho-F structure transforms into the mono-C structure and the distortion in the intralayer packing relaxes to $\epsilon_x = \epsilon_y = 2 \times 10^{-4}$. This transformation can be described by a local shear along x as shown in Fig. 2. Within the mono-C phase the displacement between adjacent layers is $s\mathbf{a}_1$, where s varies approximately linearly with temperature from 0.45 to 0.05 as shown in Fig. 4(b). The temperature dependence of s was determined from q_z scans through $\mathbf{b}_1$, as shown in Fig. 2; the peaks are located at $q_z = s$. Typical q_z scans through $\mathbf{b}_1$ and $\mathbf{b}_2$ are shown in Figs. 3(c) and 3(d), respectively. At $T = 60.02$ °C, the main peaks in Fig. 3(c) are located at $q_z = \pm 0.3$, so that $s = \pm 0.3$ at this temperature. The presence of $\pm s$ values indicates that the peaks correspond to crystallographic twins. Both twins must be present to prevent macroscopic shears from occurring; there is no net macroscopic shear in an equal mixture of the two possible shear directions. The small peaks at $q_z = \pm 0.5$ decrease in intensity as $|s|$ decreases. These remnant peaks might arise from strain-induced coexistence with the ortho-F phase or from regions of the sample where the shears go in opposite direction from one layer to the next; such an alternation would produce a unit cell containing two molecules.

At 59.75 °C, the mono-C phase transformed into the hex-AA phase, a simple hexagonal phase with AAA stacking, and the intralayer distortion vanished (within our resolution of 1×10^{-4}). This transition was indicated by a small first-order jump in s. In this phase the molecules in adjacent layers occupy sites directly above those in the layer below. Scans along q_z for the six low-order in-plane peaks are now identical to the scan in Fig. 3(d). This is the clearest evidence for the existence of an AAA-stacked hexagonal phase in the crystalline-B materials, although, Gane, Leadbetter, and Wrighton[9] previously inferred the presence of a hex-AA phase in 6O.4. This is an exceedingly rare structure in nature because it is normally unstable against a transition to one of the close-packed structures.

The ortho-F, mono-C, and hex-AA structure all have a one-dimensional modulation. As the temperature is lowered from the hcp phase, the modulation first appears at the hcp—ortho-F phase transition with a wave vector in the direction of the molecular motion (along y). As the temperature is lowered further, the modulation persists until the smectic-G phase occurs; there is a slow increase in the intensity and a slow decrease in the wave vector as the temperature is reduced. The shearing which occurs in the monoclinic phase does not appear to affect the modulation; the shearing is in the direction perpendicular to the modulation wave vector.

A careful characterization of the satellite peaks was done in the hex-AA phase of 7O.7. We found that we could produce samples in which there was a single domain of the modulated phase. Figure 5(b) shows the observed location of the peaks corresponding to the simple hexagonal lattice and of the superlattice satellite peaks produced by the modulation. The region around the (001) peak is inaccessible in our scattering geometry. High-resolution scans were done in the q_x, q_y, and q_z directions through the satellites of the (011) Bragg peak. In the x and z

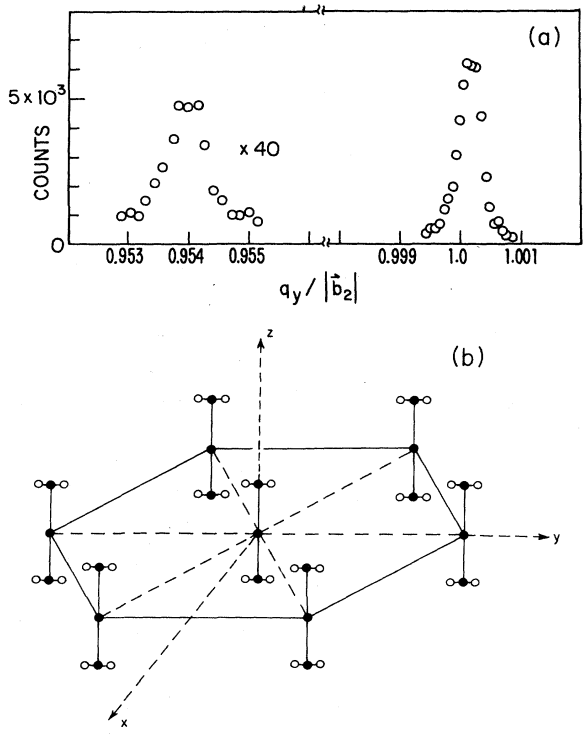

FIG. 5. (a) Synchrotron high-resolution q_y scans through the (011) peak and through its satellite in the hex-AA phase. (b) Locations of the satellite peaks. Solid circles represent the locations of the Bragg peaks corresponding to the simple hexagonal structure and the open circles indicate the locations of the satellite peaks.

directions the scans through the satellites were indistinguishable from scans through the (011) Bragg peak. The q_y scan is shown in Fig. 5(a). The FWHM of the primary peak is $4.6\times10^{-4}\,|\mathbf{b}_2|$; the satellite peak is slightly wider, indicating a correlation length for the modulation of $\sim$4000 Å. At this temperature the wave vector of the modulation was $\mathbf{Q}_m=0.046\mathbf{b}_2$, corresponding to a modulation wavelength of about 95 Å. Although this was not a commensurate wave vector, it was very close to $\mathbf{b}_2/22$. As the temperature was lowered, the modulation wave vector gradually decreased to $0.038\mathbf{b}_2$ just above the transition to the smectic-G phase, corresponding to a gradual modulation-wavelength increase to about 115 Å. The resolution of the modulation-wave-vector measurements was not sufficient to determine whether it decreases continuously or had discrete jumps.

As in the previous measurements,[11–13] no satellites were observed in the $q_z=0$ plane indicating that the polarization of the modulation is perpendicular to the plane of the smectic layers. The amplitude of the modulation was determined from the intensity relative to the primary peak of the simple hexagonal lattice and the polarization was determined from the systematic extinction of the $q_z=0$ satellites. The relative intensity for a weak-modulation satellite peak is given by

$$I_{\text{sat}}=I_{\text{Bragg}}(\tfrac{1}{2}\mathbf{q}\cdot\mathbf{u})^2\,, \tag{1}$$

where $\mathbf{q}$ is the scattering vector and $\mathbf{u}$ is the amplitude of the sinusoidal modulation; the modulation must be very nearly sinusoidal because of the absence of any detectable higher-order satellites. In the $q_z=2\pi/c$ plane the satellite intensities are given by

$$I_{\text{sat}}=I_{\text{Bragg}}\left[\frac{\pi u_0}{c}\right]^2, \tag{2}$$

where u_0 is the amplitude of the modulation and c is the layer spacing. The measured intensity ratio $I_{\text{sat}}/I_{\text{Bragg}}\sim2\%$ at $T=59\,^\circ\text{C}$ indicated an amplitude $u_0=0.05c$. Near the transition to the smectic-G phase, the intensity ratio increased to about 8% indicating that the amplitude doubled, so $u_0=0.1c$.

Another unusual feature of crystalline-B materials is the intense diffuse scattering that is observed. Both hydrodynamical theory[19] and light-scattering measurements[20] indicate that there are two sets of modes which have much lower frequencies than the rest of the modes. The first set of low-frequency modes have their wave vectors normal to the smectic layers and their polarizations in the plane of the layers. Scattering from these modes produces the intense diffuse scattering observed in a q_z scan through $\mathbf{b}_1$ or $\mathbf{b}_2$. Our measurements of this scattering for the hcp, ortho-F, and hex-AA phases are shown in Fig. 6. The data in the hex-AA phase was taken with much better vertical resolution; the factor of 20 increase in the vertical resolution is responsible for the observed decrease in the diffuse intensity for the hex-AA phase. The peaks at half-integral q_z positions in Fig. 6(b) and the peaks at integral q_z positions in Fig. 6(c) are present because we did not have a single-domain sample. Because $|\mathbf{b}_1|<|\mathbf{b}_2|$, we could separate the two ridges quite well

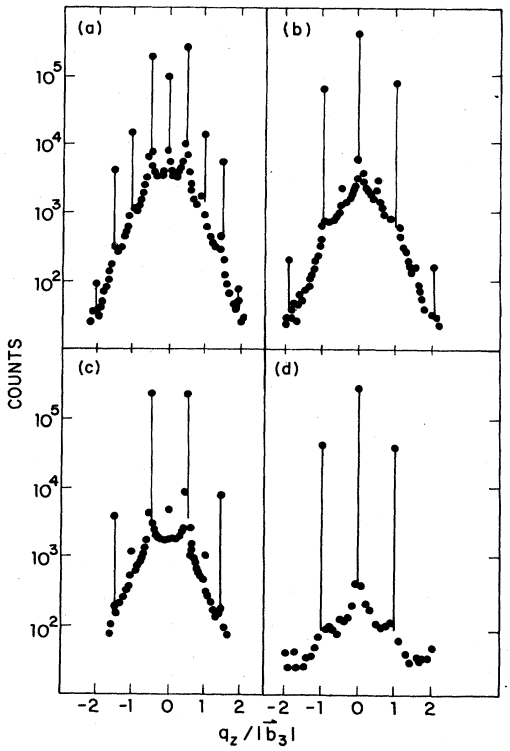

FIG. 6. High-resolution q_z scans illustrating the diffuse scattering characteristic of crystalline-B materials. Vertical lines through the Bragg points are guides for the eye. (a) hcp structure at $T=66\,^\circ\text{C}$. (b) ortho-F structure through $\mathbf{b}_2$ at $T=62\,^\circ\text{C}$. (c) ortho-F structure through $\mathbf{b}_1$ at $T=62\,^\circ\text{C}$. (d) hex-AA phase at $T=57\,^\circ\text{C}$.

with high resolution; however, the tails of the resolution function extended far enough along the ridge to pick up some scattering from the nearby Bragg peak. The envelope of the Bragg intensities and of the diffuse scattering are given by the product of the Debye-Waller factor and the molecular form factor. The observed envelopes for each phase (corrected for the resolution) superimpose nicely, indicating that these modes are largely unaffected by the phase transitions.

The second set of low-frequency modes are layer-undulation modes. These modes are polarized normal to the smectic layers and propagate in the plane of the layers. In the hex-AA phase, these modes produce a scattering intensity in the region between the Bragg peak and the satellite peak in the $q_z=2\pi/c$ plane which is about $\frac{1}{500}$ of the Bragg intensity (measured at higher resolution). This intensity is comparable to the intensity of the diffuse ridges produced by the first set of low-frequency modes.

IV. DISCUSSION

Several of the features of this sytem merit further discussion. The simple hexagonal structure with one molecule per unit cell is an exceedingly rare structure since it is usually unstable and transforms to one of the more stable close-packed structures. However, the presence of the

sharp satellite peaks in this phase indicates that it actually has a more complicated structure. The hex-*AA* stacking is presumably stabilized by the modulation.

The second point that should be emphasized is that the structures found here are not unique to 7O.7. Evidence for layer modulations exists in every compound in the homologous *n*O.*m* N-(4-*n*-alkoxybenzylidene)-4'-(*n*-alkyl)anilines series which has a crystalline-*B* phase just above a smectic-*G* or a smectic-*F* phase.[12,13] It is very likely that the modulated phases previously identified as hcp structures are actually ortho-*F* structure; we have also studied 5O.6 and have shown that the phase which had been identified as a modulated hcp is, in fact, an ortho-*F* structure.[16,21] Moncton and Pindak[6] reported some single domain data on the crystalline-*B*-phase restacking transitions in 4O.8 which strongly suggest that the two lowest-temperature phases they observed correspond to the ortho-*F* and mono-*C* phases identified here.

Two pieces of evidence suggest that molecular tilt is one of the important driving factors in the restacking transitions observed here. The first is that all the crystalline-*B* phases, except the hcp, are modulated. The modulation grows in amplitude as the transition to the tilted smectic-*G* phase is approached. This trend has been noted in other systems with modulated *B* phases and suggests that the modulated phases are a precursor to the tilted phases which lie at lower temperatures. The second point is that the displacements of the molecules within a given layer with respect to their neighbors is similar to the displacements which occur when the molecules tilt with respect to the layer normals. The amplitude and wavelength of the modulation correspond to a nearest-neighbor displacement of about 2% of the molecular length at the low-temperature end of the hex-*AA* phase. This should be compared with an 8% displacement in the lower-temperature smectic-*G* phase.

The fact that all the structures which are not close packed have the associated modulation suggests that the modulation plays a fundamental role in stabilizing these structures. This stabilization has been explained by a dislocation-mediated model[22] for the restacking transitions which occur in 7O.7. This model accounts for the non-close-packed structures by a dislocation-induced tilting of the layers. The spontaneous ordering of the dislocations into an ordered array explains both the symmetry of the phases and the amplitude of the observed modulations. The only free parameter in the model is the modulation wave vector which is set equal to the measured wave vector; the in-plane lattice spacing of the dislocation array is equal to the modulation wavelength, but the lattice spacing is a very delicate function of the dislocation interactions and cannot be calculated easily. This model also provides an excellent description of the observed restacking transitions in 5O.6

This study has shown that the behavior of bulk samples (thick films) of these weakly coupled 2D crystalline systems is extremely rich. Recent studies of thin films of 7O.7 have shown that there are radical changes in the phase diagram as a function of the film thickness.[21,23] Two tilted hexatic phases, the smectic-*F* and smectic-*I* phases, are introduced between the crystalline-*B* and the smectic-*G* phases in very thin films. The smectic-*F* phase first appears over a narrow temperature range when the film thickness is reduced to about 180 layers and then gradually widens its temperature range as the thickness is reduced further. The smectic-*I* phase first appears at a lower film thickness (about 25 layers) and also gradually widens as the thickness is reduced. The surface interactions evidently destabilize the untilted crystalline phases and stabilize the tilted hexatic phases; this is consistent with the known tendency of the molecules in these materials to tilt at the film surface[24] and reemphasizes the importance of the tilt degree of freedom in determining the phase transitions of these materials. We are currently studying the phase transitions of these weakly coupled 2D hexatics and the crossover to truly 2D systems (two-layer films). The phase transition behavior of these remarkable hexatics appear to be as rich as the behavior already observed in the crystalline systems. Finally, it is clear that much more theoretical and experimental work is needed on these unusual quasi-2D systems.

Note added in Proof. Recent experiment results by Eric Sirota and P.S.P. indicate that on cooling the ortho-*F* phase the one-dimensional modulation breaks up into a two-dimensional structure. In addition, the modulation in the hex-*AA* and mono-*C* phases is shown to be two dimensional.

ACKNOWLEDGMENTS

This work was supported by the National Science Foundation under Grant No. NSF-DMR-82-12189 and No. DMR-80-20247 and from the Danish National Science Foundation. Support for foreign travel for J.C., P.S.P., and J.A.-N. was provided by a NATO Research Grant. In addition, Dave Litster participated in the HASYLAB measurements displayed in Figs. 4(a), 5(a), and 6. We gratefully acknowledge both his assistance and his permission to publish the results in the present format. Participation of Bob Birgeneau in an early form of this work is also gratefully acknowledged.

*Present address: IBM Corporation, Department 242/040-2, Rochester, MN 55901.

†Present address: Department of Physics, University of Washington, Seattle, WA 98195.

[1]D. R. Nelson and B. I. Halperin, Phys. Rev. B **19**, 2457 (1979).

[2]P. G. de Gennes and G. Sarma, Phys. Lett. **38A**, 219 (1972).

[3]B. A. Huberman, D. M. Lublin, and S. Doniach, Solid State Commun. **17**, 485 (1975).

[4]R. J. Birgeneau and J. D. Litster, J. Phys. (Paris) Lett. **39**, L399 (1978).

[5]A. M. Levelut, J. Doucet, M. Lambert, J. Phys. (Paris) **35**, 773 (1974). A. de Vries, A. Ekachai, and N. Spielberg, J. Phys. (Paris) Colloq. **40**, C3-147 (1975); A. Leadbetter, J. Frost, J. P. Gauglan, and M. A. Mazid, J. Phys. (Paris) Colloq. **40**, C3-185 (1975); J. Doucet, A. M. Levelut, and M. Lambert, Ann. Phys. (N.Y.) **3**, 157 (1978); J. Doucet and A. M. Levelut, J.

Phys. (Paris) **38**, 1133 (1977).
[6]D. E. Moncton and R. Pindak, Phys. Rev. Lett. **43**, 701 (1979).
[7]P. S. Pershan, G. Aeppli, J. D. Litster, and R. J. Birgeneau, Mol. Cryst. Liq. Cryst. **67**, 205 (1981).
[8]D. E. Moncton and R. Pindak, in *Ordering in Two Dimensions: Proceedings of an International Conference Held at Lake Geneva, U.S.A.,* edited by S. K. Sinha (North-Holland, New York, 1980), pp. 83—90.
[9]P. A. C. Gane, A. J. Leadbetter, and P. G. Wrighton, Mol. Cryst. Liq. Cryst. **66**, 247 (1981).
[10]R. Pindak, D. E. Moncton, J. W. Goodby, and S. C. Davey, Phys. Rev. Lett. **46**, 1135 (1981).
[11]A. J. Leadbetter, J. C. Frost, and M. A. Mazid, J. Phys. (Paris) **40**, 325 (1979).
[12]A. J. Leadbetter, M. A. Mazid, and B. A. Kelly, Phys. Rev. Lett. **43**, 630 (1979).
[13]A. J. Leadbetter, M. A. Mazid, and R. M. Richardson, in *Liquid Crystals,* edited by S. Chandrasekhar (Cambridge University Press, London, 1980), pp. 65—79.
[14]J. Thoen and G. Seynhaeve (unpublished).
[15]J. Collet, L. B. Sorensen, P. S. Pershan, R. J. Birgeneau, J. D. Litster, and J. Als-Nielsen, Phys. Rev. Lett. **49**, 553 (1982).
[16]Jeffrey Allen Collett, Ph.D. thesis, Harvard University, 1983.
[17]C. Y. Young, R. Pindak, N. A. Clark, and R. B. Meyer, Phys. Rev. Lett. **40**, 773 (1978).
[18]Index of refraction values were assumed to be approximately the same as those published for 4O.8 by P. S. Pershan, in *The Molecular Physics of Liquid Crystals,* edited by G. R. Luckhurst and G. W. Gray (Academic, New York, 1979), p. 365.
[19]P. C. Martin, O. Parodi, and P. S. Pershan, Phys. Rev. A **6**, 2401 (1972).
[20]Y. Liao, N. A. Clark, and P. S. Pershan, Phys. Rev. Lett. **30**, 639 (1973).
[21]Jeffrey Collett, P. S. Pershan, E. B. Sirota, and L. B. Sorensen (unpublished).
[22]John Hirth, P. S. Pershan, J. Collett, E. B. Sirota, and L. B. Sorensen, Phys. Rev. Lett. **53**, 473 (1984).
[23]Jeffrey Collett, P. S. Pershan, E. B. Sirota, and L. B. Sorensen, Phys. Rev. Lett. **52**, 356 (1984).
[24]C. Rosenblatt, R. Pindak, N. A. Clark, and R. B. Meyer, Phys. Rev. Lett. **42**, 1220 (1979).